# Nitrogenated porous carbon electrodes for supercapacitors

**Betzaida Batalla Garcia · Stephanie L. Candelaria ·
Guozhong Cao**

**Abstract** Nitrogenated porous carbon materials, made by
coating the pore surface with nitrogen functional groups
from the pyrolysis of hexamine, were characterized and
tested for supercapacitor applications. From X-ray photo-
electron spectroscopy, the nitrogen content of the nitro-
genated carbon sample was found to be 14 wt%.
Electrochemical properties from potentiostatic and galva-
nostatic measurements, and open circuit voltage (OCV)
were used to evaluate the effect of nitrogen in porous carbon
electrodes. The nitrogenated carbon exhibits pseudocapac-
itive behavior and an increase in capacitance that is almost
double that of plain porous carbon. The cyclic stability is
also improved, as the sample retains its high capacitance
even after extensive cycling. Also, the nitrogenated carbon
shows battery-like characteristics with an initial OCV of ca.
0.4 V, and an OCV of ca. 0.3 V after cycling.

## Introduction

Modifying carbon with nitrogen functional groups or
nitrogen dopants is considered a valuable method to
increase the conductivity, even when it is electrically
insulating (like amorphous $sp^3$ carbon) [1]. Some mecha-
nisms that are known to enhance the conductivity and
charge storage of carbon include bond structure, active
redox sites, and delocalization of charge (ions or electrons)
[2–5]. An example can be seen in supercapacitors that use
an aqueous electrolyte to promote redox reactions [2],

where the capacitance is up to three times larger than that
of electric double-layer supercapacitors (EDLS) [2–5].
While redox reactions are responsible for the pseudoca-
pacitance in aqueous electrolytes, in organic electrolytes,
other mechanisms can be present. These mechanisms
include the conjugation of the carbon functional groups,
Lewis base or acid interaction, and polaron formation. All
these mechanisms create a pseudocapacitive behavior
similar to that seen in conducting polymers [6].

Synthesis of nitrogen-rich carbon focuses on either
incorporating nitrogen heteroatoms into the porous carbon
network or functionalizing the surface of the carbon with
nitrogen-containing molecules [7]. Various methods exist
for introducing nitrogen heteroatoms into carbon. In one
method, a gas rich in nitrogen is used to introduce nitrogen
functional groups after carbonization or activation of the
carbon. In this case, wet chemistries are also used to increase
the surface functionality [8, 9]. However, this method can be
time-consuming or involve the use of dangerous chemical
processes. Another method uses a nitrogen-rich polymer,
such as melamine resin, as a precursor to provide dopants
before pyrolysis. Although this is effective at low tempera-
tures, at the high pyrolysis temperature necessary to produce
glassy carbons (ca. 1000 °C), nitrogen in cyclic structures
decomposes into $N_2$ [3, 10]. This is an issue as pyrolysis at a
lower temperature can leave unwanted functional groups.

To introduce nitrogen-containing molecules onto the
pore surface of porous carbon, different methods can be
used. One such method is chemical modification. For
example, ammonia borane has been added to carbon
hydrogels during solvent exchange for hydrogen storage
applications. This chemical modification was shown to
increase the surface area (SA) and produce a larger mes-
opore volume when compared to unmodified carbon [11].
Other methods focus on modifying with nitrogen after

B. B. Garcia · S. L. Candelaria · G. Cao (✉)
Department of Materials Science and Engineering,
University of Washington, 302 Roberts Hall, Seattle,
WA 98195-2120, USA
e-mail: gzcao@u.washington.edu

pyrolysis and activation so as not to change the underlying carbon structure. These include the addition of conductive polymers, such as polyaniline, polypyrrol, and polythiopene [12–16]. However, special care must be taken to avoid blocking the carbon pores with the polymer during deposition [14]. Another method is sublimation of nitrogen-containing molecules like those used in this study. In a previous study by Kawaguchi et al. [17], 2,3,6,7-tetracyano and 1,4,5,8-tetraazanaphthalene were sublimated into the porous material to add nitrogen-rich functional groups. However, the processing temperature was >600 °C. This high temperature reduced the effectiveness of the nitrogen adsorption, removing functional groups like (iso)cyanide compounds that can contribute to pseudocapacitive behavior. It is worth noting that most of these studies also have a goal of increasing the oxygen content to promote redox reactions in aqueous systems. Few have tested the performance in organic electrolytes [9].

With hexamethylenetetramine, or hexamine, a similar effect seen in the study of Kawaguchi et al. can be obtained through its pyrolytic decomposition. Hexamine decomposes through pyrolysis into heterocyclic and aliphatic structures rich in nitrogen and (iso)cyanic compounds [18]. Its adamantine structure produces a stable solid that can sublimate at room temperature. This aspect allows for the use of a wide range of temperatures during processing, unlike using nitrogen-containing polymers that require high temperatures to sublimate [17]. The wide range of temperatures can also provide a variety of functional groups. For example, molecules that are weakly bonded to the carbon, like (iso)cyanic compounds, are allowed to remain in the structure. Another advantage of hexamine is the lack of oxygen as part of its molecular structure, preventing the redox reactions that degrade organic electrolytes.

Although the use of nitrogen functional groups is intended to increase the charge storage of carbonaceous materials (amorphous carbon, ordered mesoporous carbon, and even carbon nanotubes), hexamine derived nitrogen functional groups can be utilized in other applications as well. One proposed application is to boost the capacitance of electrodes by the controlled release or activation of such molecules. To obtain this effect, the hexamine products can be confined into the micropores and mesopores, using the hierarchy of pore size as a sieving mechanism.

In this study, nitrogenated carbon materials were made by coating the internal surface of porous carbon with nitrogen compounds from the pyrolysis of hexamine (from here on referred to as CN). These materials were then tested for supercapacitor applications. Electrochemical properties from potentiostatic and galvanostatic measurements, and open circuit voltage (OCV) were used to evaluate the effect of the nitrogen in the CN electrode. The chemical composition and structure were tested using

X-ray photoelectron spectroscopy (XPS), measuring both the nitrogen adsorbed and its effect in the porous structure.

## Experimental

### Synthesis

Porous carbon samples were prepared following a procedure reported by Wu et al. [19]. Resorcinol, furaldehyde, and hexamine were purchased from Sigma-Aldrich and used as received. The furaldehyde to resorcinol (FR) molar ratio was set to 2.5 and the resorcinol to hexamine (RH) molar ratio was set to 50. In general, the resorcinol and furaldehyde were mixed together first, followed by the addition of solvent (mixtures of *tert*-butyl alcohol and water in this case) and finally hexamine as the catalyst. The mixture was stirred after each addition. The samples were gelled in an oven at 80 °C for 7 days, then dried under vacuum at −50 °C in a Labconco FreeZone 1 L freeze dryer. Pyrolysis was performed under $N_2$ at a temperature of 900 °C for 180 min, with a ramp rate of 5 °C/min. For the sublimation of hexamine, 1 mol of the carbon sample was mixed with 1 mol of hexamine. The powder mixture was heated in a covered container under $N_2$ to 500 °C for 180 min, using a ramp rate of 25 °C/min. This temperature was chosen because it is well above the temperature at which hexamine sublimates (280 °C), but not high enough to induce sintering in the carbon.

### Composition and SA analysis

All XPS spectra were taken on a Surface Science Instruments S-probe spectrometer. This instrument has a monochromatized Al X-ray source and a low energy electron flood gun for charge neutralization. X-ray spot size for these acquisitions was $800 \times 800$ μm. All samples were run as insulators meaning that charge neutralization was used. Pressure in the analytical chamber during spectral acquisition was about $5 \times 10^{-9}$ Torr. Pass energy for survey spectra (composition) was 150 eV. Data analysis was carried out using the Service Physics ESCA 2000A analysis program (Service Physics, Bend OR). The take-off angle (the angle between the sample normal and the input axis of the energy analyzer) was 55°, corresponding to a sampling depth of approximately 50–70 Å.

The nitrogen sorption analysis was performed using a Quantachrome NOVA 4200e. The total SA was determined using the multipoint Brunauer–Emmett–Teller (BET) method. The Barrett–Joyner–Halenda (BJH) method was used to determine the mesopore SA, pore volume, pore diameter, and size distribution. The Dubinin–Astakhov (DA) method was used to determine the same properties in

the micropore region. This includes the micropore size distribution, a limiting factor in the electrolyte penetration.

Electrochemical analysis

Electrodes were prepared by grinding the samples into a fine powder then mixing with 3 wt% polytetrafluoroethylene (PTFE) to act as a binder. The resulting electrodes had a thickness of 80 μm and a diameter of 10 mm. To test the electrodes, an asymmetrical two-electrode test cell was constructed with the nitrogenated carbon as the working electrode and unmodified carbon as the counter and reference electrode. A three-electrode test cell was also constructed to test the contribution from the nitrogenated carbon only. A Celgard® porous film separated the electrodes, and to reduce the interfacial effect, specially coated aluminum contacts were used. The electrochemical test cell was assembled and sealed under an argon-rich environment (ca. 70 % Ar according to glove box manufacturer PlasLabs). To increase the penetration of the electrolyte into the pores, the samples were wetted three times under a -0.1 MPa vacuum. Tetraethylammonium tetrafluoroborate (TEATFB) in saturated 50/50 propylene carbonate/dimethyl carbonate was used as the electrolyte.

## Results and discussion

Composition and structure

Figure 1 and Table 1 show the XPS results from both porous carbon and nitrogenated porous carbon. The composition of nitrogen in the nitrogenated carbon sample CN was ca. 14 %, a higher percentage than that obtained by previous studies that use ammonia gas or other methods to introduce nitrogen compounds [3, 9, 10, 17]. Notice that the oxygen content in atomic weight % was ca. 3 %, which is close to the 2 % concentration of oxygen found in the pure carbon sample CC. The nitrogen signal in the CN sample had a bimodal distribution. One peak was located at the binding energy of 399 eV (usually ascribed to nitrogen in heterocyclic structures) and a second peak group was located at 397–396 eV (ascribed to (iso) cyanic groups). This composition is different from that reported in literature, which are mainly concerned with the production of heterocyclic carbon–nitrogen structures rich in oxygen [10, 20] that have binding energies greater than 400 eV. The (iso)cyanide compounds formed in the CN sample were likely from the carbon's adsorption of these species during the pyrolysis process, as carbon's porous structure is highly energetic and can adsorb a variety of molecules [21]. The (iso)cyanide groups are of the form $R{-}^{+}N{\equiv}C^{-}$ and usually break away from the R group during pyrolysis

of the material. For this reason, peaks at this level were not found in many of the literature results that use high pyrolysis temperatures for nitrogen-rich materials [17].

Structural analysis demonstrated that nitrogen adsorption leads to modifications in the structure. The sorption isotherms of the CC and CN samples looked very similar, with most of the pores in the macropore region, as shown in Fig. 2a. However, in the CN sample the desorption isotherm diverged at low relative pressures, an indication of a structural change or a chemical alteration in the mesopore and micropore regions [22]. On the other hand, the similarities of both curves suggest that the structure of the porous carbon is still present. The fact that the structure is preserved makes the nitrogen modification process described here suitable for other types of porous carbon structures, like ordered mesoporous carbons [10, 20, 23].

Figure 3 compares the pore size distribution of porous carbon and nitrogenated carbon samples. A marked decrease of the micropore volume is seen, which is caused by micropores filling with nitrogen groups, while little change in the mesopore volume is observed. The micropore size increases slightly from 1.2 to 1.68 nm. This is another indication that the micropores might be filled, leaving only the larger pores accessible to $N_2$ adsorption. This mechanism is illustrated in Fig. 2b. The filling of the micropores and mesopores is best observed by measuring the pore volume. Table 2 shows that the micropore volume of the CN sample disappears, suggesting that the nitrogen compounds are mostly entrapped in the micropores. This can be explained by the increased surface energy due to the high curvature of the micropores [22]. This is a known natural phenomenon and is behind the behavior of capillary forces and the relaxation of confined molecules [22, 24, 25]. The SA of the samples supports this finding. The CN sample had similar mesopore and macropore areas as compared to the CC sample (each retaining 88 and 75 % of the area, respectively) while no micropore area was detected. Furthermore, the density of the CN and CC samples correlated with the sorption isotherm data. While the CC sample had a density of only 0.6 g/cc, the CN sample had a density of 0.9 g/cc. This increase in density can be attributed to the adsorbed nitrogen.

In summary, the adsorption of nitrogen molecules only affected the available SA for the electric double-layer (EDL) formation in the micropore region, while not dramatically affecting larger pores. This structural and chemical modification of the CN carbon will later serve as a control mechanism to access the active molecules in the micropores, increasing its capacitance while cycling.

Pseudocapacitance and current density

The CN electrodes showed no redox peaks in the cyclic voltammograms but have pseudocapacitive behavior. In

**Fig. 1** XPS data for **a** CN and **b** carbon. Corrected position of the *1s* peaks for **c** carbon and **d** nitrogen
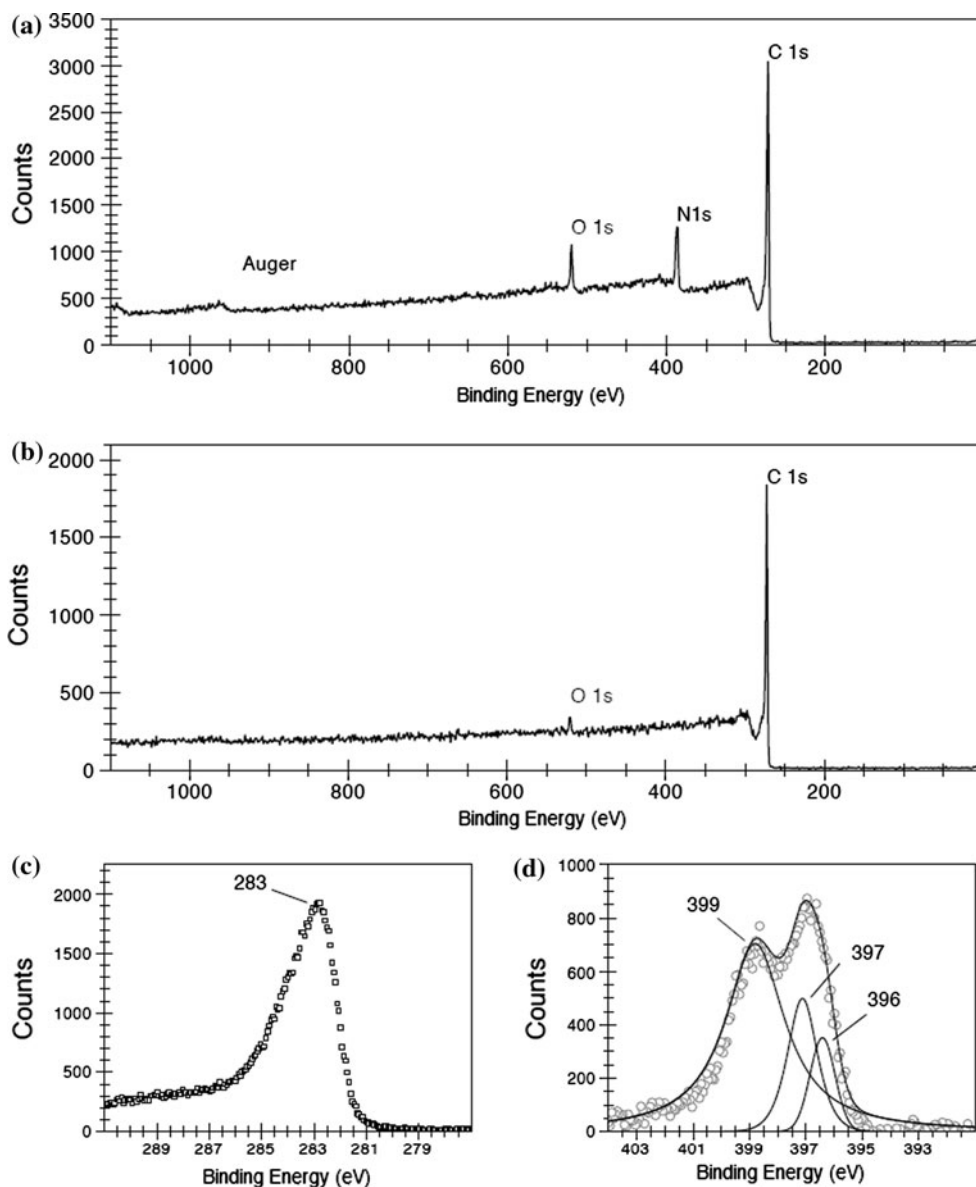


**Table 1** Compositional data from XPS

| Sample ID | C Atomic % | O | $N_{Total}$ | $N_{HC}$ | $N_{IC}$ |
|---|---|---|---|---|---|
| CC | 98.2 | 1.8 | – | – | – |
| CN | 82.6 | 3.2 | 14.1 | 9.6 | 4.5 |

$N_{HC}$ nitrogen in heterocyclic group, $N_{IC}$ isocyanic group

Fig. 4, two tests were used to analyze an asymmetric capacitor composed of a CN working electrode and a CC counter electrode. The CC electrode is used to avoid an active material in the counter electrode. First, the samples were tested using a two-electrode test cell, which is how the capacitors are utilized in practice. The cyclic voltammograms in Fig. 4 show a nearly squared cycle profile that is characteristic of porous electrodes. In the first few

cycles, a strong peak is present at the 2 V potential and disappears after cycling. After cycling the device 10,000 times and remeasuring the average current density, the current is nearly unchanged. This is a highly desirable trait in supercapacitors when used in applications such as automobiles [26, 27], which require frequent charge and discharge cycles.

To study the CN electrode in more detail, an additional capacitor using the same asymmetric setup was tested using a three-electrode test cell, as shown in Fig. 4b. This setting provides a more accurate value of the specific capacitance since the contribution from the large SA CC electrode was removed. The current density of the three-electrode setup is further increased compared to the two-electrode setup. Although the strong peak at 2 V indicates that pseudocapacitance is present, there are no

**Fig. 2 a** Isotherms of the CN and CC samples. Both isotherms have similar shape at P/P0 > 0.3, indicating similar mesoporous structure. Micropores experienced the most drastic change in volume. **b** Schematic of pore filling with nitrogen molecules
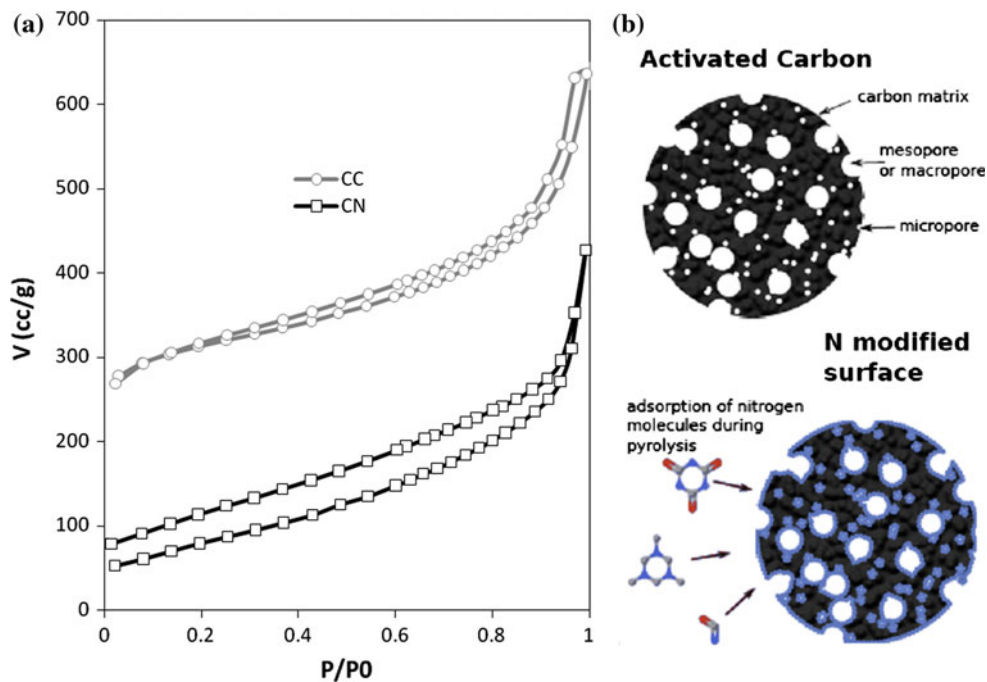


**Fig. 3** Pore size distributions. **a** BJH desorption distribution, showing only a small difference between the mesopores in the CC sample and the CN sample. **b** DA micropore distribution, showing the increase in pore size and decrease in micropore volume when comparing CC to CN
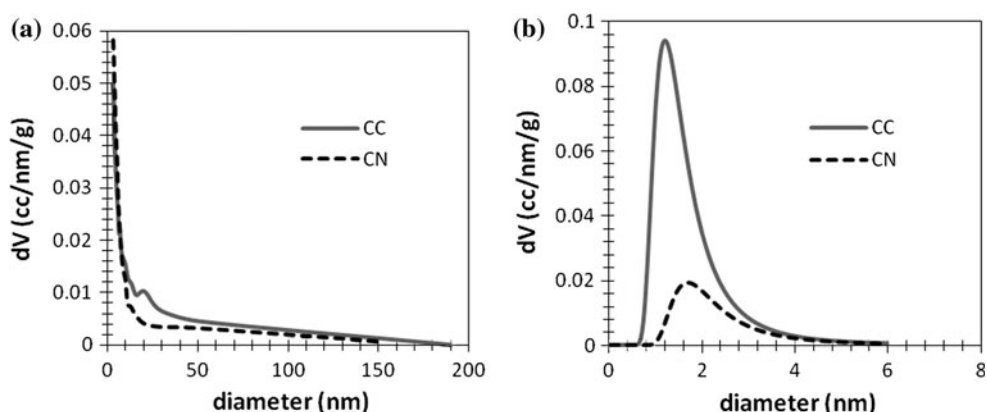


**Table 2** Nitrogen sorption data for pure carbon (CC) and nitrogenated carbon (CN)
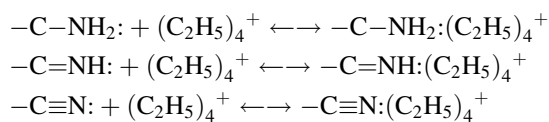
| Sample ID | $S_{BET}$ m²/g | $S_{Micro}$ | $S_{Meso}$ | $S_{Macro}$ | $V_{Micro}$ cc/g | $V_{Meso}$ | $D_{Micro}$ nm | $D_{Meso}$ |
|---|---|---|---|---|---|---|---|---|
| CC | 934 | 635 | 193 | 128 | 0.35 | 0.30 | 1.20 | 3 |
| CN | 290 | 0 | 171 | 97 | – | 0.30 | 1.68 | 3 |

$S_x$ surface area, $V_x$ pore volume, $D_x$ pore diameter

other obvious peaks (like those seen for redox reactions in batteries) below 2 V.

This absence of redox peaks while cycling is an indication that there is another mechanism present in the nitrogenated carbon that contributes pseudocapacitance, but the exact mechanism is unknown at the time. However, one proposed explanation is faradic reactions [28], induced by lone electron pairs from the nitrogen groups interacting with the cations in the electrolyte. The following are possible reactions that could be taking place on the nitrogenated carbon surface:

$$-C-NH_2: + (C_2H_5)_4^+ \longleftrightarrow -C-NH_2:(C_2H_5)_4^+$$
$$-C=NH: + (C_2H_5)_4^+ \longleftrightarrow -C=NH:(C_2H_5)_4^+$$
$$-C\equiv N: + (C_2H_5)_4^+ \longleftrightarrow -C\equiv N:(C_2H_5)_4^+$$
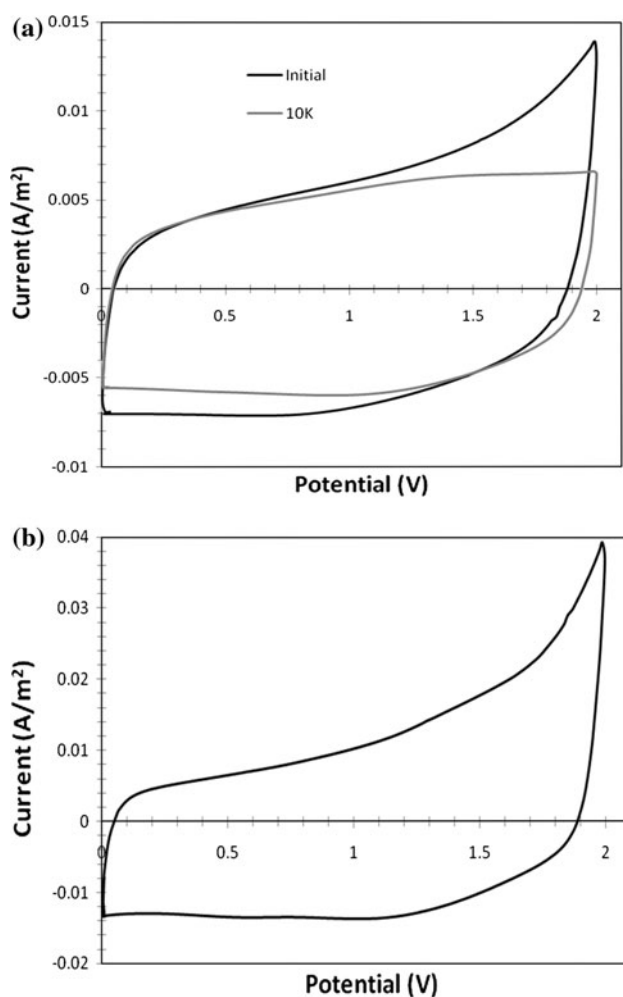
Fig. 4 Cyclic voltammograms of nitrogenated carbon using **a** 2- and **b** 3-electrode cells. The *black line* is the initial sample and the *gray line* is the sample after 10,000 cycles

## Capacitor endurance and capacitance gain

As is typical with unmodified carbon, there is a loss in capacitance for the CC electrode after cycling. After 1,000 cycles, the capacitance of the CC device drops by approximately 22 %. However, the CN device experiences only a modest loss in capacitance after 1,000 cycles. It drops by just 5 %. The differences in cycling behavior between the two samples are even more dramatic when the devices are cycled 10,000 times. This can be seen in Fig. 5, where the CC device experiences increased discharge slopes at both high current densities (5 mA/cm$^2$, Fig. 5a) and low current densities (0.5 mA/cm$^2$, Fig. 5b). The CN electrode, on the other hand, retained its current density, and hence its charge, as the supercapacitor was cycled extensively. One scenario that can explain this is that the nitrogen is helping to reduce the aging of the electrolyte [29]. However, the galvanic cycles suggest that the nitrogen functional groups were being activated with capacitor cycling. The resulting

effect can be seen in Figs. 5c, d. After cycling the electrode 10,000 times at a high current density of 5 mA/cm$^2$, the capacitor experienced only a modest loss in the capacitance, expressed in Fig. 5c as an increased discharge slope. However, the active material is still within the small micropores. At a low current density of 0.5 mA/cm$^2$, the capacitance increased after 10,000 cycles (a reduction in the discharge slope, shown in Fig. 5d), i.e., more charge was generated as the device was cycled. This mechanism can provide a way to compensate for the loss of capacitance seen in the purer carbon electrodes. Notice that the pseudocapacitiance effect can be seen when the CN electrode is measured using a three-electrode test cell (Fig. 5e, f). This effect was not noticeable in the two-electrode setup.

## Battery-like behavior

### Increased charge storage

Because the SA of the devices is different, the capacitance was also normalized to the BET SA. The SA normalized capacitance of the CN device was almost twice that of the CC device. Figure 6 demonstrates this difference when comparing the curves for CC and CN (3-electrode). The CN sample was tested using a three-electrode test cell to measure only the contribution from the CN electrode. When using a two-electrode test cell, the capacitance of the asymmetric CN device decreased due to the contribution from the CC electrode ($1/C_{Total} = 1/C_{CN} + 1/C_{CC}$). In the asymmetric capacitor, the high capacitance was shown to remain at lower voltage rates (large $1/\sqrt{v}$) after the capacitor was cycled 10,000 times. This retention is not seen in the CC sample, as the capacitance is lower after 10,000 cycles. Furthermore, the specific power of the CN sample also increases after cycling, whereas the CC sample's power decreases significantly.

One explanation is that during cycling, the active material is slowly depleted, starting with the larger pores (both macropores and mesopores), and then moving on to the micropores. This is similar to a controlled time release process, which is activated by the potential cycling. In addition, the combined effect of the incremental exposure of the underlying carbon surface and pseudocapacitance can explain why the capacitance increased after cycling 10,000 times. Surface modification like that seen in this CN sample can be applied to a variety of high SA electrodes to extend the life of the capacitor with minimal charge losses.

### Self-generated potential

The OCV is the potential generated between the working and counter electrode when a zero current is applied (also

**Fig. 5** Galvanic cycles for unmodified carbon cycled at **a** 5 and **b** 0.5 mA/cm², and nitrogenated carbon showing **c** a loss of capacitance during discharge at 5 mA/cm², and **d** gain of capacitance at 0.5 mA/cm². The *black line* is the initial cycle and the *gray line* is after 10,000 cycles. **e**, **f** represent initial galvanic cycles of the 3-electrode test cell at 5 and 0.5 mA/cm², respectively
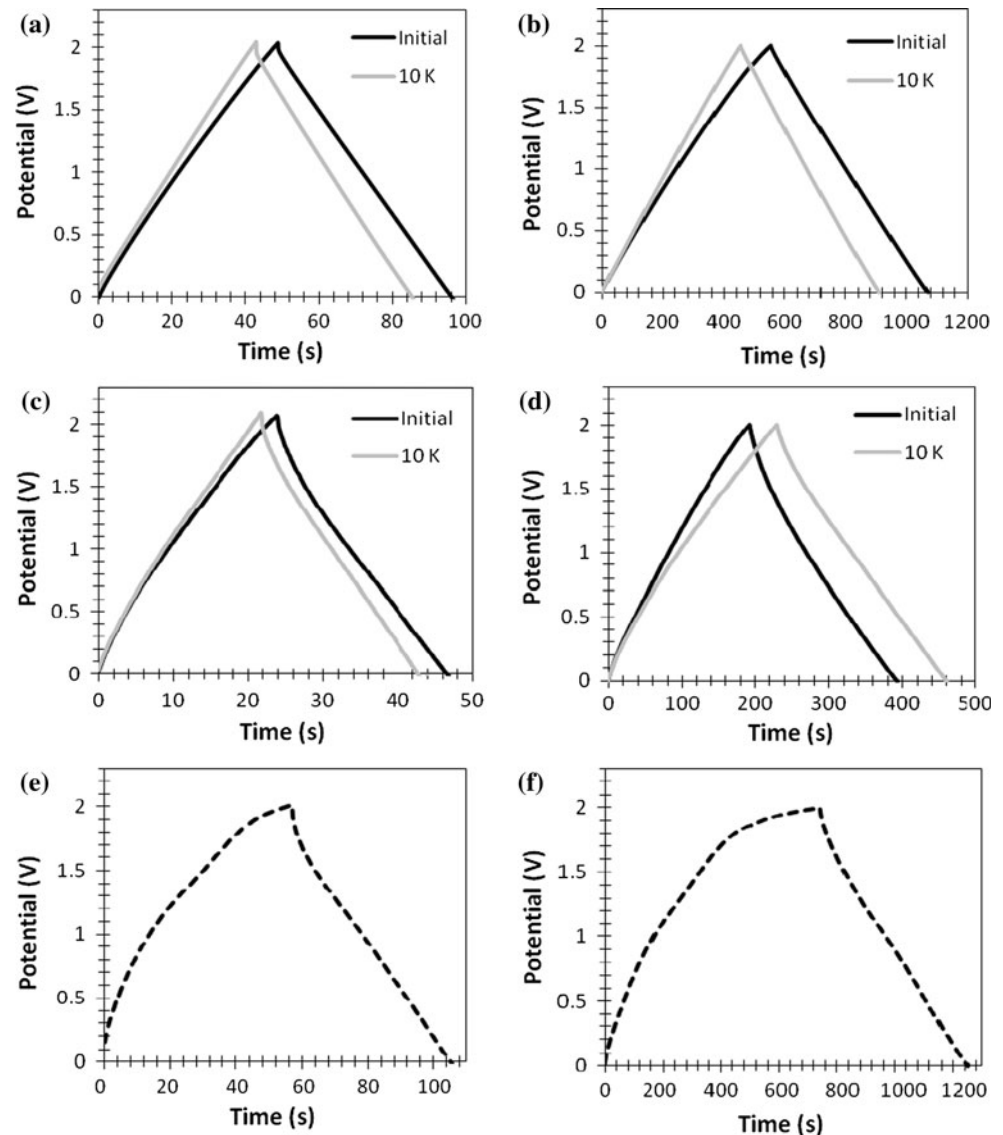


known as corrosion potential). Unlike the carbon electrodes that have an OCV of nearly zero, the CN sample can reach voltages of up to 0.4 V. This is a clear indication of changing surface chemistry with nitrogen modification. The OCV of the CN sample was tested under three different scenarios: (1) under initial conditions, (2) after setting the cell voltage to zero or complete discharge then recovery, and (3) after cycling the capacitor 50 times then zeroing the voltage or discharging the device and recovery. Under initial conditions as shown in Fig. 7a, the test results showed that the OCV is approximately 0.4 V. When the capacitor voltage is set to zero for an hour and then the OCV is measured, the voltage increased to 0.25 V. If the same capacitor subsequently cycled 50 additional cycles and remeasured from the 0 V potential, there is still ca. 0.1 V remaining. Notice that during this initial series of cycles, the OCV saturates with time. However, the important aspect is

that a net potential was generated only by the introduction of nitrogen functional groups.

After cycling the capacitor for 10,000 times, the recovery of the OCV experienced a few changes, as seen in Fig. 7b. Following the three scenarios outlined above, after 10,000 cycles, the OCV remained at 0.3 V. After zeroing the voltage, the OCV reduced slightly from that measured initially to 0.15 V. After a 50 cycle test and zeroing the potential, the OCV increased further to ca. 0.2 V. Unlike the saturation observed in the initial experiments, the slope of the OCV potential continued to increase. One explanation of this positive net potential is that the nitrogen contains one more electron than carbon, making it more polarized. Therefore, nitrogenated carbon may have a higher surface charge density than unmodified carbon, meaning that it can accommodate more charges per unit SA. This high OCV is characteristic of battery systems,
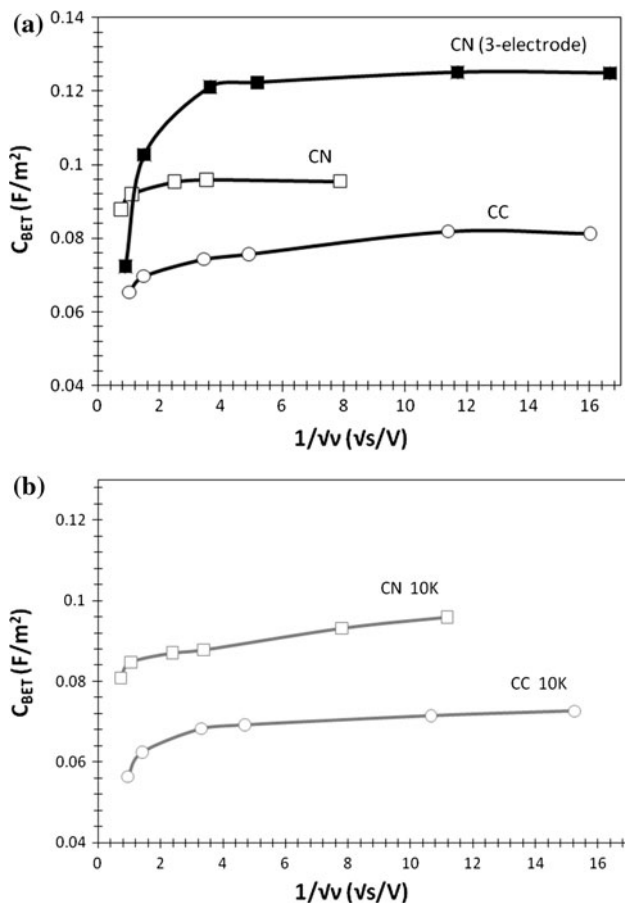
**Fig. 6** Capacitance as a function of $1/\sqrt{v}$ for samples **a** initially and **b** after 10,000 cycles. The capacitance of the nitrogenated carbon electrode is almost twice that of the plain carbon. The asymmetric capacitor, tested with a two-electrode test cell, has capacitance values that lie between the plain carbon and the nitrogenated carbon due to series capacitance



**Fig. 7** OCV for the CN sample as a function of time for **a** initial cycles and **b** after 10,000 cycles. (*1*) OCV of original sample, (*2*) after setting the voltage to zero, and (*3*) after 50 cycles setting the voltage to zero. Notice the saturation in the curves for the initial cycles. The *dashed line* represents the OCV for plain carbon

giving the CN supercapacitor battery-like characteristics. Again, it is also a clear indication of a change in surface chemistry of the nitrogenated carbon as compared to unmodified carbon. Additional studies are underway to further understand the mechanisms behind this phenomenon.

## Conclusion

The pyrolytic decomposition of hexamine has been demonstrated to be a viable method to modify the surface chemistry of carbon. The results show a nitrogen composition that includes (iso)cyanide groups in addition to heterocyclic structures. The introduced compounds are adsorbed into the porous carbon, especially in the micropores. The capture of the nitrogen molecules in the micropores produces a controlled release or activation of such functional groups when a potential is applied or
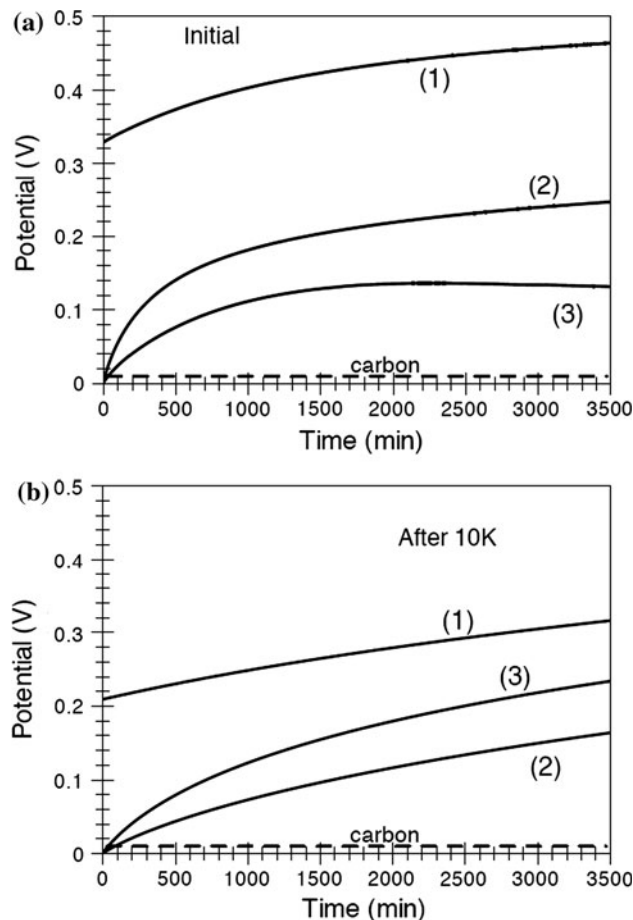
cycled. The nitrogen compounds provide the carbon with pseudocapacitive properties that enhance the carbon. These enhancements include high cycle life stability, increased charge and current density (produced by pseudocapacitance of the nitrogen compounds), and battery-like characteristics with an OCV of ca. 0.3 V after extensive cycling.

## References

1. Silva SRP (2003) Properties of amorphous carbon. INSPEC, London
2. Ania CO, Khomenko V, Raymundo-Pinero E, Parra JB, Beguin F (2007) Adv Funct Mater 17:1828

3. Jiang J, Gao Q, Xia K, Hu J (2009) Micropore Mesopore Mat 118:28
4. Lota G, Grzyb B, Machnikowska H, Machnikowski J, Frackowiak E (2005) Chem Phys Lett 404:53
5. Zheng LP, Wang Y, Wang XY, Wang XY, An HF, Yi LF (2010) J Mater Sci 45:6030. doi:10.1007/s10853-010-4687-x
6. Xu G, Wang W, Qu X, Yin Y, Chu L, He B, Wu H, Fang J, Bao Y, Liang L (2009) Eur Polym J 45:2701
7. Frackowiak E (2006) J Braz Chem Soc 17:1074
8. Jurewicz K, Babel K, Ziolkowski A, Wachowska H (2003) Electrochim Acta 48:1491
9. Hulicova-Jurcakova D, Kodama M, Shiraishi S, Hatori H, Zhu ZH, Lu GQ (2009) Adv Funct Mater 19:1800
10. Li W, Chen D, Li Z, Shi Y, Wan Y, Wang G, Jiang Z, Zhao D (2007) Carbon 45:1757
11. Sepehri S, Garcia BB, Zheng Q, Cao GZ (2009) Carbon 47:1436
12. Tamai H, Hakoda M, Shiono T, Yasuda H (2007) J Mater Sci 42:1293. doi:10.1007/s10853-006-1059-7
13. Frackowiak E, Beguin F (2001) Carbon 39:937
14. Chen WC, Wen TC, Teng H (2003) Electrochim Acta 48:641
15. Lei Z, Chen Z, Zhao XS (2010) J Phys Chem C 114:19867
16. Wu M, Snook GA, Gupta V, Shaffer M, Fray DJ, Chen GZ (2005) J Mater Chem 15:2297
17. Kawaguchi M, Itoh A, Yagi S, Oda H (2007) J Power Sources 172:481
18. Ullmann F, Gerhartz W, Yamamoto YS, Campbell FT, Pfefferkorn R, Rounsaville JF (2007) Ullmann's Encyclopedia of Industrial Chemistry. VCH, Deerfield Beach
19. Wu D, Fu R, Zhang S, Dresselhaus M, Dresselhaus G (2004) J Non-Cryst Solids 336:26
20. Kim W, Kang MY, Joo JB, Kim ND, Song IK, Kim P, Yoon JR, Yi J (2010) J Power Sources 195:2125
21. Pierson HO (1993) Handbook of carbon, graphite, diamond and fullerenes—properties, processing and applications. William Andrew Publishing/Noyes, Park Ridge
22. Lu GQ, Zhao XS (2004) Nanoporous materials science and engineering. Imperial College Press, London
23. Lota G, Lota K, Frackowiak E (2007) Electrochem Commun 9:1828
24. Garcia BB, Feaver AM, Champion RD, Zhang Q, Fister TT, Nagle KP, Seidler GT (2008) J Appl Phys 104:014305
25. Brinker CJ, Scherer GW (1990) Sol-gel science: the physics and chemistry of sol-gel processing. Academic Press, Boston
26. Lukic SM, Cao J, Bansal RC, Rodriguez F, Emadi A (2008) IEEE Trans Ind Electron 55:2258
27. Burke AF (2007) Proc IEEE 95:806
28. Frackowiak E (2007) Phys Chem Chem Phys 9:1774
29. Azais P, Duclaux L, Florian P, Massiot D, Lillo-Rodenas MA, Linares-Solano A, Peres JP, Jehoulet C, Beguin F (2007) J Power Sources 171:1046